A New High Resolution Scheme for the Solution of the Compressible Navier-Stokes Equations

Shigefumi Tatsumi

Mitsubishi Heavy Industries, Ltd., Nagoya Aerospace Systems Works
Nagoya, Japan

Abstract

A new flux splitting and limiting technique which yields one-point stationary shock capturing is presented. The technique is applied to the full Navier-Stokes and Reynolds Averaged Navier-Stokes equations. Calculations of laminar boundary layers at subsonic and supersonic speeds are presented together with calculations of transonic flows around airfoils. the results show very good agreement with theoretical solutions or existing experimental data. It is shown that the proposed scheme improves the resolution of viscous flows while maintaining one-point shock capturing property.

1. Introduction

The calculation of compressible viscous flows requires schemes which could not affect the global accuracy of the solution of the *physical* viscous problem though they should be *numerically* dissipative enough on the other hand. Recently a large class of schemes including High Resolution Switched schemes, Symmetric Limited Positive (SLIP), and Upstream Limited Positive (USLIP) schemes has been analyzed.[5,13] SLIP and USLIP schemes were implemented and tested using several forms of flux-splitting including scalar, characteristic, and Convective Upwind and Split Pressure (CUSP) schemes. Careful comparisons with analytical results for laminar boundary layers clearly indicate that the limiting process plays a greater role than the flux-splitting in determining the quality of viscous results. However, new trade-offs between the different forms of flux-splitting arise whenever crisp resolution of shocks becomes important.

Roe has shown that characteristic splitting can yield an optimal discrete shock resolution with only one interior point.[10] More recently Jameson has shown that a discrete shock structure with a single interior point can be supported by artificial diffusion which both produces an upwind flux for the flow determined to be supersonic and satisfies a generalized eigenvalue problem for the exit from the shock. These two conditions can be satisfied by both the characteristic and CUSP schemes whereas scalar diffusion fails to satisfy the first condition.

The present work focuses on the CUSP based schemes which combine perfect one-point shock capturing of stationary shocks with high resolution of boundary layer properties.

2. Formulations

2.1 Convective Upwind and Split Pressure (CUSP)

For simplicity we consider the general one dimensional conservation law for a system of equations which can be expressed as

$$\frac{\partial w}{\partial t}+\frac{\partial}{\partial x}f(w)=0. \tag{1}$$

Here the following are the state and flux vectors.

$$w=\begin{pmatrix}\rho\\ \rho u\\ \rho E\end{pmatrix},\quad f=\begin{pmatrix}\rho u\\ \rho u^2+p\\ \rho u H\end{pmatrix} \tag{2}$$

If γ is the ratio of specific heats and c is the speed of sound, then

$$p=(\gamma-1)\rho(E-\frac{u^2}{2})$$

$$c^2=\frac{\gamma p}{\rho}$$

$$H=E+\frac{p}{\rho}=\frac{c^2}{\gamma-1}+\frac{u^2}{2}$$

In a steady flow H is constant. This remains true for the discrete scheme only if the numerical diffusion is constructed so that it is comparable with this condition.

The conservation law (1) is approximated on a mesh with an interval Δx by the semi-discrete scheme

$$\Delta x\frac{dw_j}{dt}+h_{j+1/2}-h_{j-1/2}=0, \tag{3}$$

and the numerical flux can be taken as the following equation.

$$h_{j+1/2}=\frac{1}{2}(f_{j+1}+f_j)-d_{j+1/2} \tag{4}$$

$d_{j+1/2}$ is a diffusive flux which is introduced to enable the scheme to resolve discontinuities without producing oscillations in the discrete solution.

Suppose that the first order diffusive flux is defined as a combination of differences of the state and flux vectors

$$d_{j+1/2}=\frac{1}{2}\alpha^*_{j+1/2}c(w_{j+1}-w_j)+\frac{1}{2}\beta_{j+1/2}(f_{j+1}-f_j). \tag{5}$$

Schemes of this class are fully upwind in supersonic flow if one takes $\alpha_{j+1/2}$=0 and $\beta_{j+1/2}$=sign(M) when the absolute value of the local Mach number satisfies $|M|>1$. In order to support a stationary discrete shock structure with a single interior point, α^* and β cannot be chosen independently. It turns out that once α^* is chosen, β is uniquely determined by the equilibrium at the exit of the shock, leading to a one parameter family of schemes satisfying the relation

$$\alpha^*=(1+\beta)(1-M)$$

when $M>1$. The choice $\beta=M$ corresponds to the Harten-Lax-Van Leer (HLL) scheme, which is extremely diffusive. We will develop schemes of this class based on a decomposition of the flux vector f. If the convective terms are separated by splitting the flux according to the following equations (6) and (7), then the total effective coefficient of convective diffusion is expressed as (8),

$$f=uw+f_p,\ \text{where}\ f_p=\begin{pmatrix}0\\ p\\ up\end{pmatrix} \tag{6}$$

$$f_{j+1}-f_j=\bar{u}(w_{j+1}-w_j)+\bar{w}(u_{j+1}-u_j)+f_{p_{j+1}}-f_{p_j} \tag{7}$$

$$\alpha c=\alpha^* c+\beta\bar{u} \tag{8}$$

where $\bar{u}$ and $\bar{w}$ are arithmetic averages.

The choice of $\alpha c=\bar{u}$ leads to low diffusion near a stagnation point, and also leads to a smooth continuation of convective diffusion across the sonic line since $\alpha^*=0$ and β=1 when $|M|$>1. The scheme must also be formulated so that the cases of u>0 and u<0 are treated symmetrically. Using the notation M=u/c and $\lambda^{\pm}=u\pm c$, this leads to the diffusion coefficients

$$\alpha=|M|,\ \beta=\begin{cases}+\max(0,\dfrac{u+\lambda^-}{u-\lambda^-}) & \text{if } 0\le M\le 1\\ -\max(0,\dfrac{u+\lambda^+}{u-\lambda^+}) & \text{if } -1\le M\le 0\\ sign(M) & \text{if } |M|\ge 1.\end{cases} \tag{9}$$

Near a stagnation point α may be modified to $\alpha=\frac{1}{2}(\alpha_0+\frac{M^2}{\alpha_0})$ if $|M|$ is smaller than a threshold α_0.

Equation (9) remains valid when CUSP scheme is modified to

allow solutions with constant stagnation enthalpy. The coefficients α(M) and β(M) are displayed in figure 1 for the case of $\alpha_0 = 0$. The cutoff of β when $|M| < 1/2$, together with α approaching zero as $|M|$ approaches zero, is also appropriate for the capture of contact discontinuities.

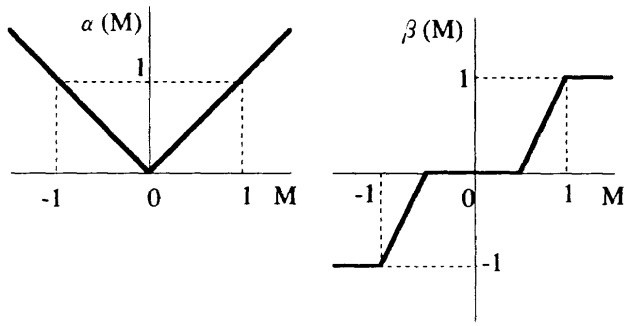

Figure 1: Coefficients of the scheme

An important property of this scheme is that it has lower diffusion than the standard characteristic upwind scheme, which can be illustrated by introducing a Roe linearization and by rewriting the diffusive flux as

$$d_{j+1/2} = \frac{1}{2}(\alpha^* cI + \beta A_{j+1/2})(w_{j+1} - w_j). \quad (10)$$

Introducing the characteristic decomposition, the diffusive flux can now be represented as

$$d_{j+1/2} = RMR^{-1}(w_{j+1} - w_j) \quad (11)$$

The matrix M is diagonal with eigenvalues $\mu_1 c$, $\mu_2 c$, $\mu_3 c$ displayed in figure 2.

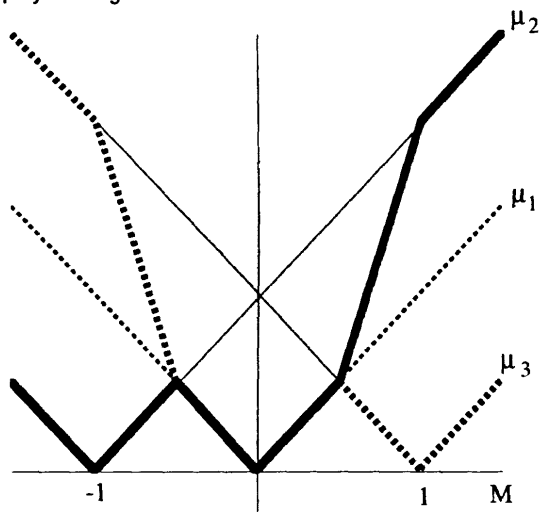

Figure 2: Eigenvalues of diffusion matrix

Strict positivity is not enforced, but at a shock

$$\Delta f = A\Delta w = S\Delta w$$

where S is the shock speed. Thus Δw must be an eigenvector corresponding to one of the eigenvalues $u \pm c$, and positivity is enforced for the corresponding characteristic variable.

2.2 H-CUSP Formulation

In steady flow the stagnation enthalpy H is constant, corresponding to the fact that the energy and mass equations are consistent when the constant factor H is removed from the energy equation. Discrete and semi-discrete schemes do not necessarily satisfy this property. In the case of a semi-discrete scheme expressed in viscous form - equations (3) and (4) - a solution with constant H is admitted if the viscosity for the energy equation reduces to the viscosity for the continuity equation with ρ replaced by ρH.

In order to extend the CUSP formulation to allow for isenthalpic solutions, we introduce the linearization

$$f_R - f_L = A_h(w_{h_R} - w_{h_L})$$

where w_h is a modified state vector with ρH replacing ρE. The matrix A_h may be calculated in the same way as the standard Roe linearization. In particular, by introducing the vector

$$v = \begin{pmatrix} \sqrt{\rho} \\ \sqrt{\rho}u \\ \sqrt{\rho}H \end{pmatrix}$$

all quantities in both f and w_h are products of the form $v_j v_k$ which have the property that a finite difference $\Delta(v_j v_k)$ between left and right states can be expressed as

$$\Delta(v_j v_k) = \overline{v_j}\Delta v_k + \overline{v_k}\Delta v_j$$

where $\overline{v_j}$ is the arithmetic mean $1/2(v_{jR} + v_{jL})$. Therefore,

$$\Delta w = B\Delta v, \quad \Delta f = C\Delta v = CB^{-1}\Delta w,$$

where B and C can be expressed in terms of appropriate mean values of the quantities v_j. Thus, by defining

$$u = \frac{\sqrt{\rho_R}u_R + \sqrt{\rho_L}u_L}{\sqrt{\rho_R} + \sqrt{\rho_L}}, H = \frac{\sqrt{\rho_R}H_R + \sqrt{\rho_L}H_L}{\sqrt{\rho_R} + \sqrt{\rho_L}},$$

and

$$c = \sqrt{(\gamma - 1)(H - u^2/2)},$$

it follows that

$$A_h = \begin{pmatrix} 0 & 1 & 0 \\ -\frac{\gamma+1}{\gamma}\frac{u^2}{2} & \frac{\gamma+1}{\gamma}u & \frac{\gamma-1}{\gamma} \\ -uH & H & u \end{pmatrix}.$$

The eigenvalues of A_h are u, λ^+, and λ^- where

$$\lambda^{\pm} = \frac{\gamma+1}{2\gamma}u \pm \sqrt{(\frac{\gamma+1}{2\gamma}u)^2 + \frac{c^2 - u^2}{\gamma}}.$$

Note that λ^+ and λ^- have the same sign as $u + c$ and $u - c$, respectively, and change sign at the sonic line $u = \pm c$. The corresponding left and right eigenvectors of A_h can be computed, and are given in Reference 7.

Using the modified linearization, the CUSP scheme can be reformulated as follows to admit isenthalpic steady solutions. The diffusive flux is expressed as

$$d_{j+1/2} = \frac{1}{2}\alpha^* c\Delta w_h + \frac{1}{2}\beta\Delta f,$$

where Δ denotes the difference from j+1 to j. The split is redefined as

$$f = uw_h + f_p,$$

where

$$f_p = \begin{pmatrix} 0 \\ p \\ 0 \end{pmatrix}$$

and the diffusive flux can be expressed as

$$d_{j+1/2} = \frac{1}{2}\alpha c\Delta w_h + \frac{1}{2}\beta\overline{w_h}\Delta u + \frac{1}{2}\beta\Delta f_p.$$

As before, α and β are defined by equation (9), using the modified eigenvalues $\lambda^{\pm}$ defined above.

2.3 Implementation of Limiters

In the case of scalar conservation law, high resolution schemes which guarantee the preservation of the positivity or monotonicity of the solution can be constructed by limiting the effect of higher order or anti-diffusive terms, which might otherwise cause extrema to grow. The fluxes appearing in the CUSP scheme have different slopes approaching from either side of the sonic line, and use of limiters which depends on comparisons of these fluxes can lead to a loss of smoothness in the solution at the entrance to supersonic zones in the flow.

This problem can be avoided in the implementation of the CUSP scheme by forming the diffusive flux from left and right states at the cell interface. These are interpolated or extrapolated from nearby data, subject to limiters to preserve monotonicity. In a similar manner to the reconstruction of the solution in Van Leer's MUSCL scheme[8], the following construction is used. Define the limiter

$$R(u,v) = 1 - \left| \frac{u-v}{|u|+|v|} \right|^q, \qquad (12)$$

where q is a positive power which is set equal to two in the present study. Also define the limited average

$$L(u,v) = \frac{1}{2} R(u,v)(u+v). \qquad (13)$$

Let $w^{(k)}$ denote the k th element of the state vector w. Now define left and right states for each dependent variable separately as

$$w_L^{(k)} = w_j^{(k)} + \frac{1}{2} L(\Delta w_{j+3/2}^{(k)}, \Delta w_{j-1/2}^{(k)})$$

$$w_R^{(k)} = w_{j+1}^{(k)} - \frac{1}{2} L(\Delta w_{j+3/2}^{(k)}, \Delta w_{j-1/2}^{(k)}),$$

where

$$\Delta w_{j+1/2} = w_{j+1} - w_j$$

Then

$$w_R^{(k)} - w_L^{(k)} = \Delta w_{j+1/2}^{(k)} - L(\Delta w_{j+3/2}^{(k)}, \Delta w_{j-1/2}^{(k)}), \qquad (14)$$

which in the case of a scalar equation reduces to the SLIP formulation[6].

For the CUSP schemes the pressures p_L and p_R for the left and right states are determined from w_L and w_R. Then the diffusive flux is calculated by substituting w_L for w_j and w_R for w_{j+1} to give

$$d_{j+1} = \frac{1}{2} \alpha^* c(w_R - w_L) + \frac{1}{2} \beta \{ f(w_R) - f(w_L) \}.$$

The alternative reconstruction:

$$w_L^{(k)} = w_j^{(k)} + R(\Delta w_{j+3/2}^{(k)}, \Delta w_{j-1/2}^{(k)}) \Delta w_{j-1/2}^{(k)}$$

$$w_R^{(k)} = w_j^{(k)} - R(\Delta w_{j+3/2}^{(k)}, \Delta w_{j-1/2}^{(k)}) \Delta w_{j+3/2}^{(k)}$$

has been found to yield essentially identical results for calculations of steady flows.

3. Numerical Results

Extensive numerical tests have been performed with the CUSP type schemes to verify their properties[7]. Results for inviscid flow calculated with the program FLO82 verify the one-point capturing of shocks. Examples of an inviscid result are presented in Figure 3, 4, and 5. The flow condition of freestream Mach number 0.75 and an angle of attack of 3 degrees was selected for the flow around RAE2822 airfoil. The typical O-type grid consisting of 320x64 structured grid points was used in the case. The conventional Scalar-Switch scheme[13] needs 3 internal points to form the shock wave, where the CUSP scheme needs a single point. Figure 5 shows the convergence history for Scalar-Switch and CUSP schemes. Both schemes show very rapid convergence, especially the CUSP needs only 100 multigrid cycles to achieve a final level of the averaged density residuals of the order of 10^{-11}, where the initial level is the order of 10^{-1}. In this section the results obtained for two dimensional viscous flows are mainly reported.

The calculations were performed with the program FLO103, which uses a cell-centered finite volume scheme to discretize the full Navier-Stokes equations. Time integration is carried out by a five-stage scheme which requires re-evaluation of the dissipative operators only at alternate stages[7]. This scheme couples the desirable feature of a wide stability region along both the imaginary and real axes with good high frequency damping. The efficiency of the scheme was enhanced by using an implicit averaging scheme with variable coefficients, and an effective multigrid strategy which utilizes a W-cycle.

The set of calculations presented in Figure 6 and 7 are aimed at investigating the behavior of the scheme in the supersonic regime for a flat-plate laminar boundary layer problem. Results are presented for a Reynolds number of $1x10^5$, on a grid with 32 cells in the boundary layer. They are scaled by using the Illingworth-Stewartson transformation[11], and compared with the Blasius solution. The results show that the scheme accurately reproduces the boundary layer properties in the supersonic regime.

The next test case is a turbulent boundary layer developing over a flat-plate at zero incidence. The case was chosen to investigate the behavior of the scheme for the Reynolds Averaged Navier-Stokes equations coupled with a typical turbulent model. To make comparisons as simple as possible, the well known algebraic model[1] was used in the cases. The computation results are compared with the following logarithmic formula[11].

$$\frac{u}{u_\tau} = 5.85 \log y^+ + 5.56, \; u_\tau = \sqrt{\tau_0 / \rho}, \; y^+ = y u_\tau / \nu. \qquad (15)$$

Here u, τ_0, ρ, y, and ν are tangential velocity component, wall shearing stress, density, normal distance from the wall, and kinetic viscosity respectively. The freestream Mach number of 0.15 and the Reynolds number of $1x10^7$ have been chosen for the case. Figure 8 and 9 show the results of u / u_τ in terms of $\log y^+$ using Scalar-Switch and CUSP respectively. Although the computation results don't seem to perfectly follow the self-similarity law and there are small differences between the both schemes, all the results follow the logarithmic formula in general. This fact suggests that the property of each scheme, which has been validated in laminar cases, is not much influenced by the presence of a turbulence model.

Calculations presented in Figure 11 and 12 are aimed at examining the applicability of the CUSP to laminar viscous flow problems around airfoil-like shapes. A diamond shape airfoil was chosen for the purpose. The computational grid is shown in Figure 10, where C-type grid consisting of 512x64 structured grid points is used. The freestream Mach number and an angle of attack are M_∞=3.0 and α=0 degree, respectively. $1x10^4$ and $1x10^5$ of the Reynolds number were used in the case to assume the flow is laminar. The Euler equation's case was also conducted for the comparison. Figure 11 shows the computed surface pressure distributions together with an inviscid analytical solution, where the Euler computation using CUSP nicely recovers the analytical solution. The result for Re_∞=$1x10^5$ suggests that the comparison between computed boundary layer velocity profile and the scaled Blasius solution would be meaningful since there is not much pressure gradient on the first half of the airfoil surface. Figure 12 clearly proves this hypothesis by showing that the computed tangential velocity profiles follow the self-similarity law recovering the scaled Blasius solution.

The next two cases are to examine the behavior of the CUSP scheme in practical transonic turbulent flow problems. The first one is the flow around RAE2822 airfoil with M_∞=0.75, α=3.19 deg., and Re_∞=$6.2x10^6$. The grid consists of a total of 480x64 grid points with 360 points fitted on the airfoil. Transition was fixed at the experimental location of the trip wire[3]. A Baldwin and Lomax turbulence model has been used for this case because the flow field was expected to be attached, and the behavior of the solution predicted by this model is reasonably well understood[1]. Figure 13 shows a comparison of the computed and experimental pressure distribution along the airfoil, where the agreement between them is fairy good.

The second case consists of a RC(4)-10 airfoil with M_∞=0.59 and Re_∞=$7.5x10^6$. The airfoil was designed for

application to the inboard region of a helicopter main rotor blade[9]. The turbulence model used here is again the simple algebraic one. Figure 14 shows the C-type grid consisting of a total of 512x64 grid points, which was used in th calculation. Figure 15 shows the comparison of surface pressure distribution between the computed result and experimental data at α=3.41 degrees. The agreement is very good including the shock location where the critical pressure coefficient Cp_{crit} = -1.36. The computed lift, drag, and pitching moment coefficients in terms of α are shown in Figure 16 in comparison with experimental data. The agreement is again pretty good except at higher α where steadiness of the flow is questionable.

4. Conclusions

A new flux splitting and limiting scheme has been applied to the solution of the compressible Navier-Stokes equations. The calculations performed so far indicate the scheme, which was originally tailored for non-oscillatory shock capturing, yields accurate solutions for viscous flows. It will lead an improvement of the overall computational efficiency in practical problems by allowing the use of coarser grids.

References

1. Baldwin, B. and Lomax, H., "Thin layer approximation and algebraic model for separated turbulent flow," AIAA Paper 78-257, 1978.

2. Einfeldt, B., "On Godunov-type methods for gas dynamics," *SIAM J. Num. Anal.*, 25:294-318, 1988.

3. Cook P. H., Mc Donald, M. A., and Firmin, M. C. P., "Airfoil RAE 2822 pressure distributions, Boundary layer and wake measurements," AGARD Advisory Report 138, 1979.

4. Harten, A., Lax, P. D., and Van Leer, B., "On upstream differencing and Godunov-type schemes for hyperbolic conservation laws," *SIAM Review*, 25:35-61, 1983.

5. Jameson, A., "Computational algorithms for aerodynamic analysis and design," *Appl. Num. Math.*, 13:383-422, 1993.

6. Jameson, A., "Analysis and design of numerical schemes for gas dynamics I, artificial diffusion, upwind biasing, limiters and their effect on multigrid convergence," *Int. J. Comp. Fluid. Dyn.* 1995.

7. Jameson, A., "Analysis and design of numerical schemes for gas dynamics II, artificial diffusion and discrete shock structure," *Int. J. Comp. Fluid. Dyn.* 1995.

8. Van Leer, B., "Towards the ultimate conservative difference scheme V, a second order sequel to Godunov's method," J. Comp. Phys., 32:101-136, 1979.

9. Noonan, K. W., "Aerodynamic characteristics of two rotorcraft airfoils designed for application to the inboard region of a main rotor blade," NASA-TP 3009, 1990.

10. Roe, P. L., "Fluctuations and signals - a framework for numerical evolution problems," In Morton K. W. and Baines, M. J., editors, *Proceedings of IMA Conference on Numerical Methods in Fluid Dynamics*, pp. 219-257, 1981.

11. Schlichting, H., "Boundary Layer Theory," 7th edition, McGraw - Hill, New York, 1979.

12. Tatsumi, S., Martinelli, L. and Jameson, A., "A New High Resolution Scheme for Compressible Viscous Flows with Shocks," AIAA Paper 95-0466, Jan. 1995.

13. Tatsumi, S., Martinelli, L., and Jameson, A., "Flux-Limited Schemes for the Compressible Navier-Stokes Equations," *AIAA Journal*, Vol. 33, No. 2, pp. 252-261, February 1995.

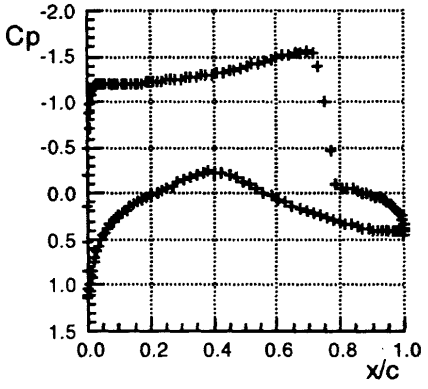

Figure 3:*Cp* distribution - Euler equations with Scalar-Switch RAE 2822 airfoil, M=0.75, α=3deg.

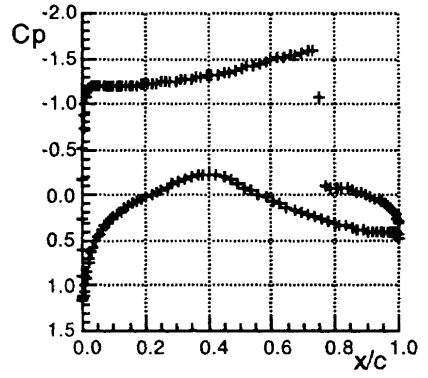

Figure 4:*Cp* distribution - Euler equations with CUSP RAE 2822 airfoil, M=0.75, α=3deg.

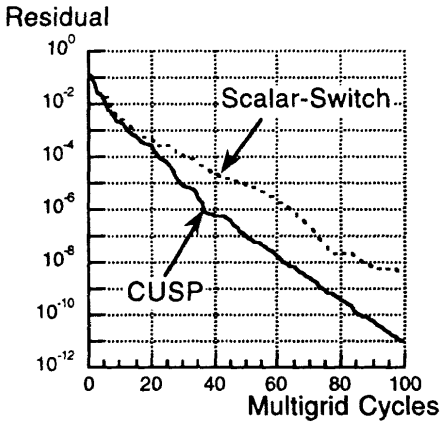

Figure 5: Convergence history - Euler equations RAE 2822 airfoil, M=0.75, α=3deg.

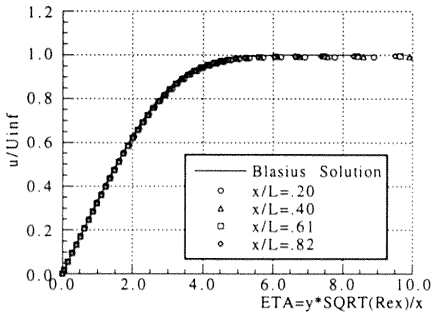

Figure 6:Flat plate laminar boundary layer tangential velocity profile at M=2.0 and Re=1x10^5 - CUSP

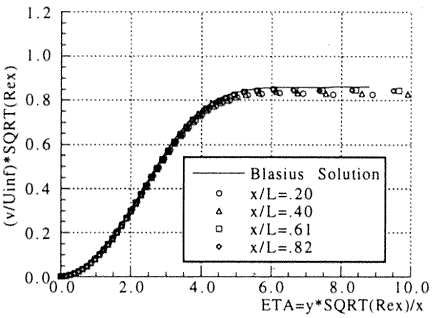

Figure 7:Flat plate laminar boundary layer transverse velocity profile at M=2.0 and Re=1x10^5 - CUSP

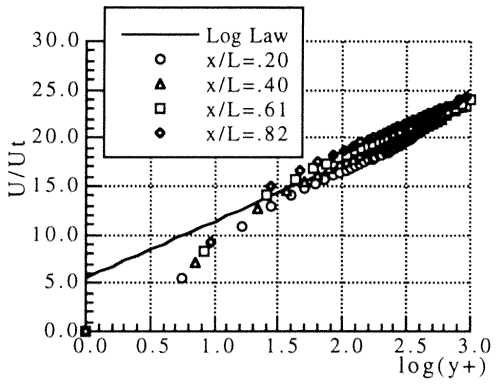

Figure 8:Flat plate turbulent boundary layer tangential velocity profile at M=0.15 and Re=1x10^7 - Scalar-Switch

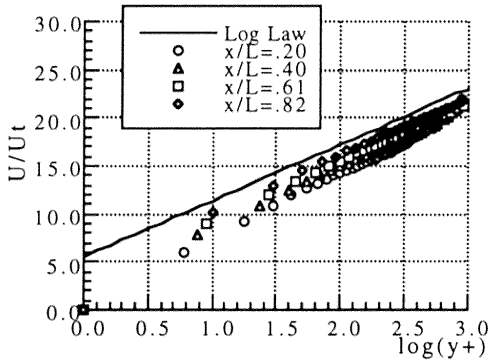

Figure 9:Flat plate turbulent boundary layer tangential velocity profile at M=0.15 and Re=1x10^7 - CUSP

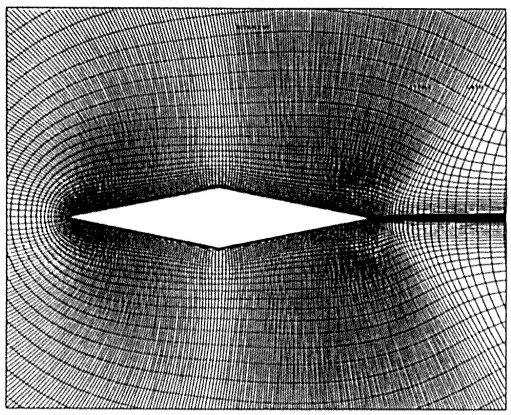

Figure 10:Computational grid for a diamond airfoil (512x64)

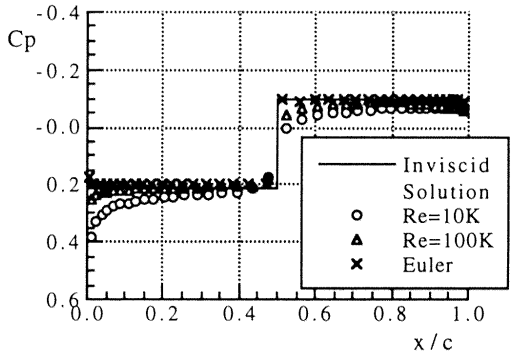

Figure 11:*Cp* distribution on a diamond airfoil at M=3.0 and α=0deg. - CUSP

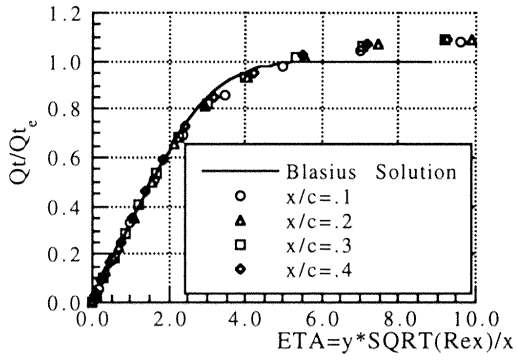

Figure 12:Laminar boundary layer tangential velocity profile on a diamond airfoil at M=3.0, α=0deg., and Re=1x10^5 - CUSP

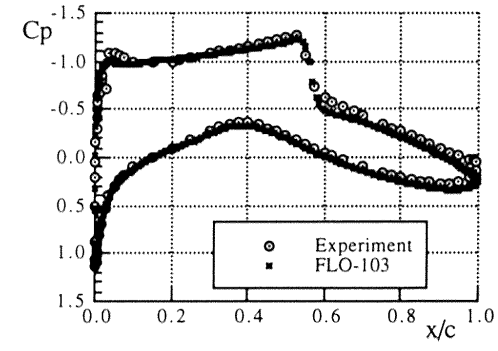

Figure 13:*Cp* distribution on RAE2822 airfoil at M=0.75, α=3.19deg., and Re=6.2x10^6 - CUSP

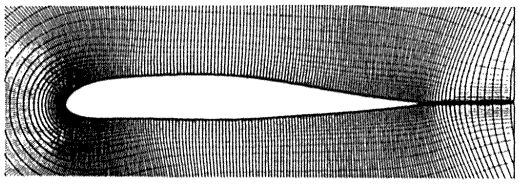

Figure 14:Computational grid for RC(4)-10 airfoil

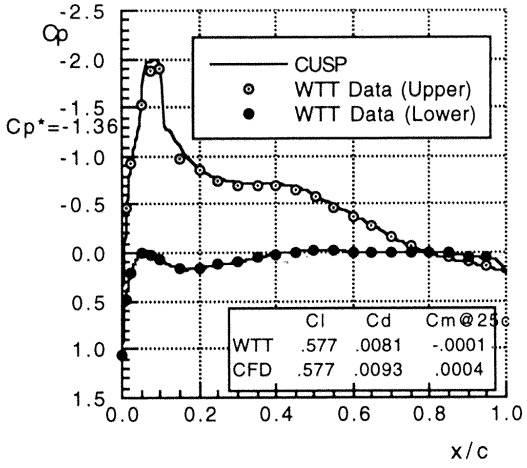

Figure 15:*Cp* distribution on RC(4)-10 airfoil
at M=0.59, α=3.41deg., and Re=7,5x10^6 - CUSP

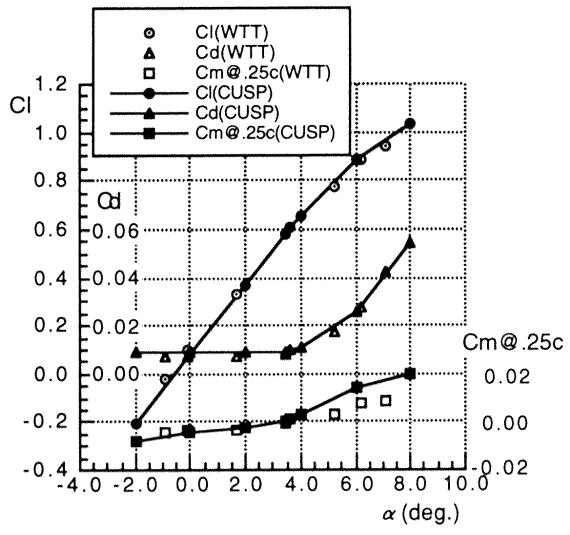

Figure 16:Comparison with experimental data for
RC(4)-10 in Cl, Cd, and Cm at M=0.59 and Re=7,5x10^6